Building confidence in CSEM for exploration - Benchmarking

Antony PRICE*, Total E&P with Claudia Twarz and Pål Gabrielsen, EMGS

Summary

Publications on the success rates, defined as predicting well outcome in frontier exploration using a combination or integration of seismic data and Controlled Source Electromagnetics (CSEM – please see Eidesmo et. al. 2002 for a description of the technique) claim rather high success rates – around 80% (Hesthammer et. al. 2012). What these publications do not detail, due possibly to confidentiality concerns is the precise methodology used, application context and how risking of targets is done numerically to make exploration and drilling decisions using these integrated data.

We discuss here the first of a series of 'benchmark' collaborative case studies using available multi-client CSEM data over existing discoveries, sub-economic discoveries and failures to better understand the predictive strength, pit-falls and failure modes of CSEM application in the exploration workflow. Clearly, the CSEM data and inversion results are not used in a vacuum – integration with all available data including seismic and well information is necessary for context and understanding of the results. Of course, collaboration across multiple stake-holders including company and contractor was required to achieve this level of integration.

The 3D CSEM benchmarks – methodology

Initially, 1D sensitivity (with pizza-box 3D target) studies were done on a range of wells to select cases where indeed CSEM would be sensitive to the presence or absence of the target. To avoid bias, the sensitivity modelling was done independently of the 3D inversion and integration work.

The CSEM data were re-calibrated and re-processed using the latest Common Source Point (CSP, all receivers within a radius share a common source position) techniques to allow an equitable comparison between data-sets of different vintage. The re-calibration using improved techniques allows access to higher frequencies along with the CSP processing advances are seen as an improvement over previous methodology bringing more efficiency and noise reduction enabling better fitting of the data in 3D inversions.

The following methodology was kept necessarily simple and realistic, with unconstrained 3D inversion of the multi-client CSEM data without reference to the details of the well results and seismic expression of the targets involved. Start models for these unconstrained inversions were simple half-space or gradient 'hung' from bathymetry with no input from the resistivity log information.

Convergence criteria for these inversions was determined qualitatively as minimization of the data fit with a maximization of model roughness (model complexity) –
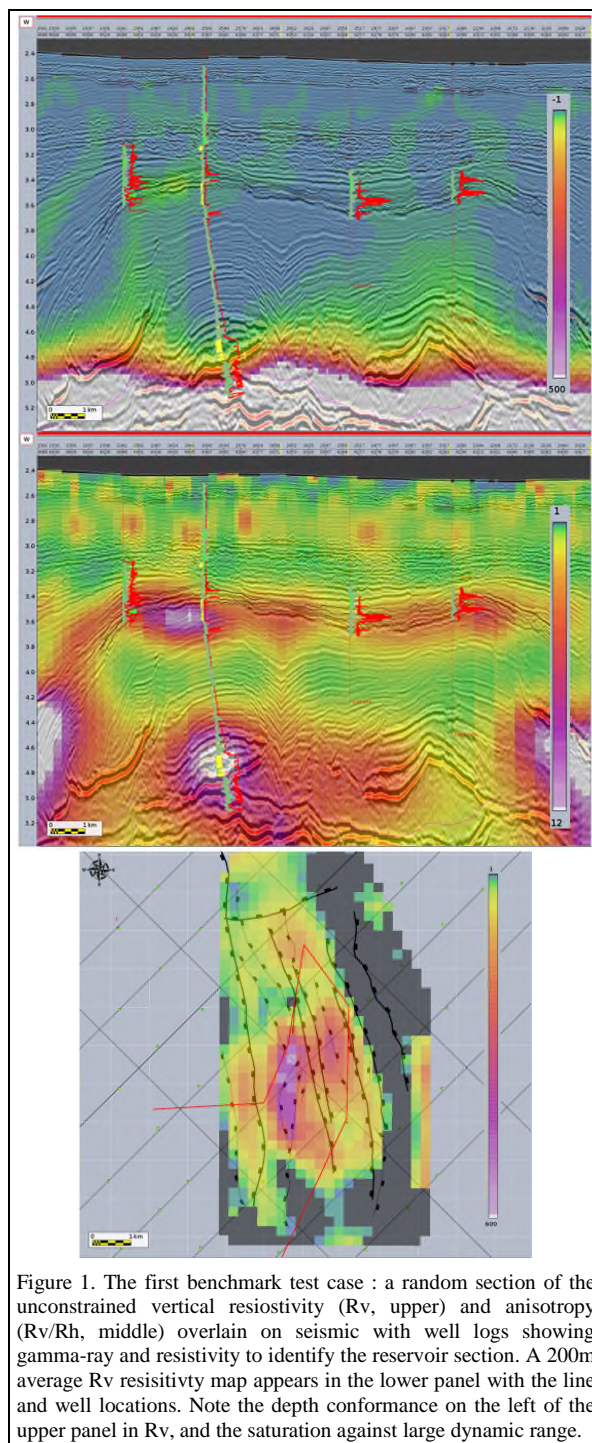

Figure 1. The first benchmark test case : a random section of the unconstrained vertical resiostivity (Rv, upper) and anisotropy (Rv/Rh, middle) overlain on seismic with well logs showing gamma-ray and resistivity to identify the reservoir section. A 200m average Rv resisitivty map appears in the lower panel with the line and well locations. Note the depth conformance on the left of the upper panel in Rv, and the saturation against large dynamic range.

that is a very 'data-driven' approach which would be the case in an exploration context pre-drill.

The codes used for inversion of the multi-client CSEM data in 3D were the L-BFGS version of CGG's software (see Rodi and Mackie 2001 for details) and EMGS's latest Gauss-Newton code along with a BFGS-TTI code where appropriate (as in Figure 2). The latter code from EMGS does require some limited information from the seismic interpretation for the variable TTI structural dips (which are free to be updated in the inversion and thus are not considered constraint) that was thought to be a reasonable addition in the context of pre-drill exploration since we normally have 3D seismic before drilling.

Contrast and comparison between different 3D CSEM inversion codes was a secondary objective for this project and was found to be additionally useful for building confidence in the stability (or uncertainty) for different inversion results. It is clearly useful to have a choice for inversion methodology to address imaging challenges in different structural and geologic contexts and to better understand the strengths and weaknesses of each code.

The 'Benchmarks'

The first 'benchmark' example in Figure 1 shows a random line through a seismic volume with the unconstrained inverted CSEM vertical resistivity (Rv, upper) anisotropy (Rv/Rh, middle) overlain. Anisotropy, which can behave somewhat as a normalization was chosen here for display due to large dynamic range of resistivity values in the background including acquisition imprints and deeper salt and volcanic structure. In this figure there are four wells intersected with gamma-ray and resistivity log curves plotted to highlight the reservoir section. Additionally, horizons in black show the multiple tops from the reservoir model. The lower panel shows a map view of a 200m average Rv resistivity with the line and well location, along with a relevant fault network at the reservoir level interpreted from the seismic data.

In both profile and map view we see quite remarkable correlation between the seismic fault mapping and well information and the CSEM Rv and anisotropy, with indications of the oil-water contact (OWC) and possibly a deeper target, sub-salt (thin layer) and hosted in vuggy carbonates illuminated in the anisotropy data that was drilled and flowed hydrocarbons (lower left).

There are indications even in these unconstrained CSEM inversions that we are seeing almost reservoir level detail when one looks at the various reservoir models and the aerial/depth distribution of upper and lower complexes.
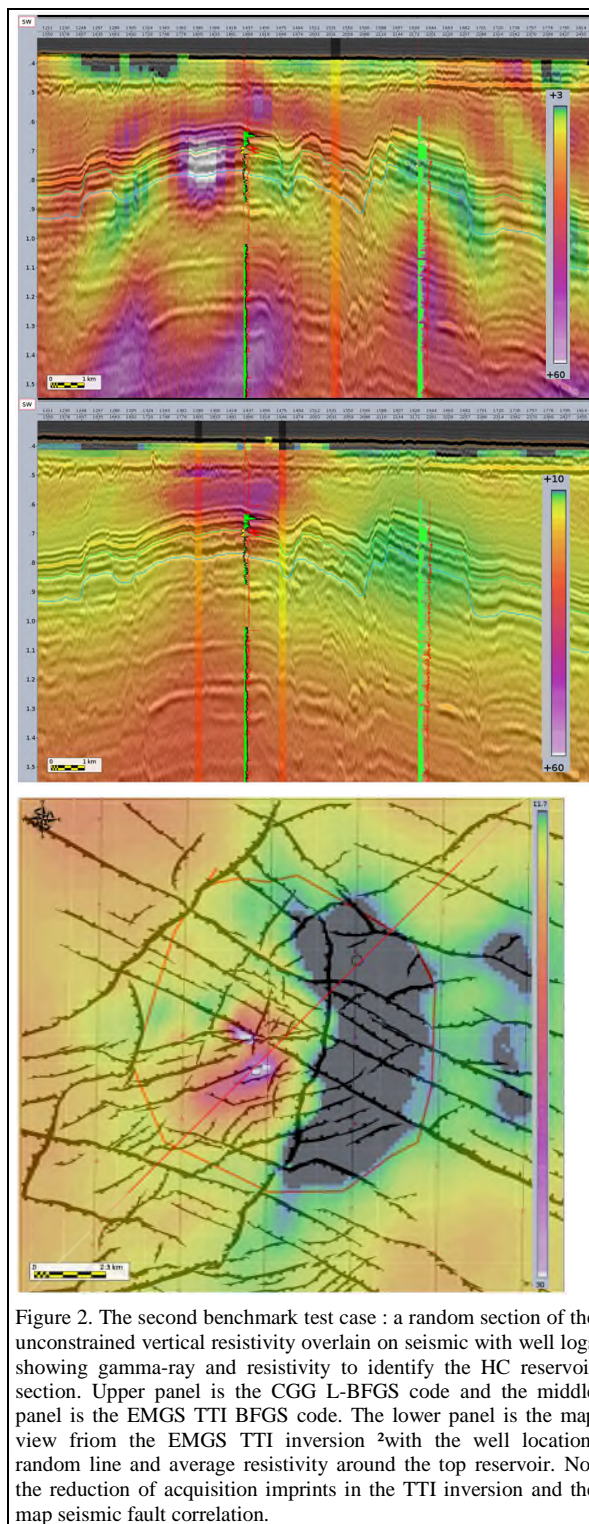

Figure 2. The second benchmark test case : a random section of the unconstrained vertical resistivity overlain on seismic with well logs showing gamma-ray and resistivity to identify the HC reservoir section. Upper panel is the CGG L-BFGS code and the middle panel is the EMGS TTI BFGS code. The lower panel is the map view friom the EMGS TTI inversion ²with the well location, random line and average resistivity around the top reservoir. Not the reduction of acquisition imprints in the TTI inversion and the map seismic fault correlation.

Figure 2 shows two wells overlain on the vertical resistivity (Rv) from the 3D CSEM inversions. In this figure, we have the leftmost well that encountered gas in the shallow section and the well to the right was water-wet with a corresponding CSEM anomaly associated with the well on the left but not on the right. Additionally, indications in the Rv display hint at fault-block compartmentalization of the gas accumulation, which is a known aspect of accumulations in this area. Rv was chosen here as opposed to the anisotropy from the previous example as the background shales are known to be highly anisotropic. This background anisotropy also magnifies the TTI effect, even though the structural dips are low.

For this reason the EMGS BFGS TTI code was tested and appears in the middle portion (and in map form in the lower portion) of Figure 2 with a clear reduction of artifacts – and a small departure from depth conformance. We feel that this example illustrates the importance of applying different CSEM inversion codes and methodology to help understand the anomalous response and build confidence in the interpretation.

Additionally, when one considers the map view of the average resistivity around the top reservoir, the fault control on gas distribution becomes clear, with a major north-south fault mapped solely in the seismic data dividing the charged and uncharged panels. Recall that these 3D CSEM inversions are unconstrained making this correlation with seismic mapped structure all the more striking.

Figure 3 displays the third test case with an example of unconstrained CSEM inversion tracking a reservoir response through a regional of shallow gas which obscures the seismic response (delineated in blue). Definition on the left for both the EMGS and CGG code inversion compares well here with the log resistivity information and seismic response, however, is slightly too shallow on the right possibly due to increased dip (>12°) and TTI effects which are known to be strong in this locality.

In general and for most of the test cases, depth conformance with respect to the seismic and well data is quite good, with some variation seen mostly attributable to BFGS methodology and some TTI effects. This improved conformance was attributed to the updated calibration techniques, the CSP re-processing, more than usual number of frequencies used (broadband data, 20 vs 5 frequencies for the first case, Figure 1), the EMGS GN inversion approach and the inclusion of the magnetic field in the BFGS inversions.

The inclusion of magnetic or H-field in the inversion problem here is seen as important where large and complex resistive structures such as salt, volcanics and possibly anisotropic background appear to be better resolved with the additional data – possibly due to constructive stacking of the co-varying E and H fields.
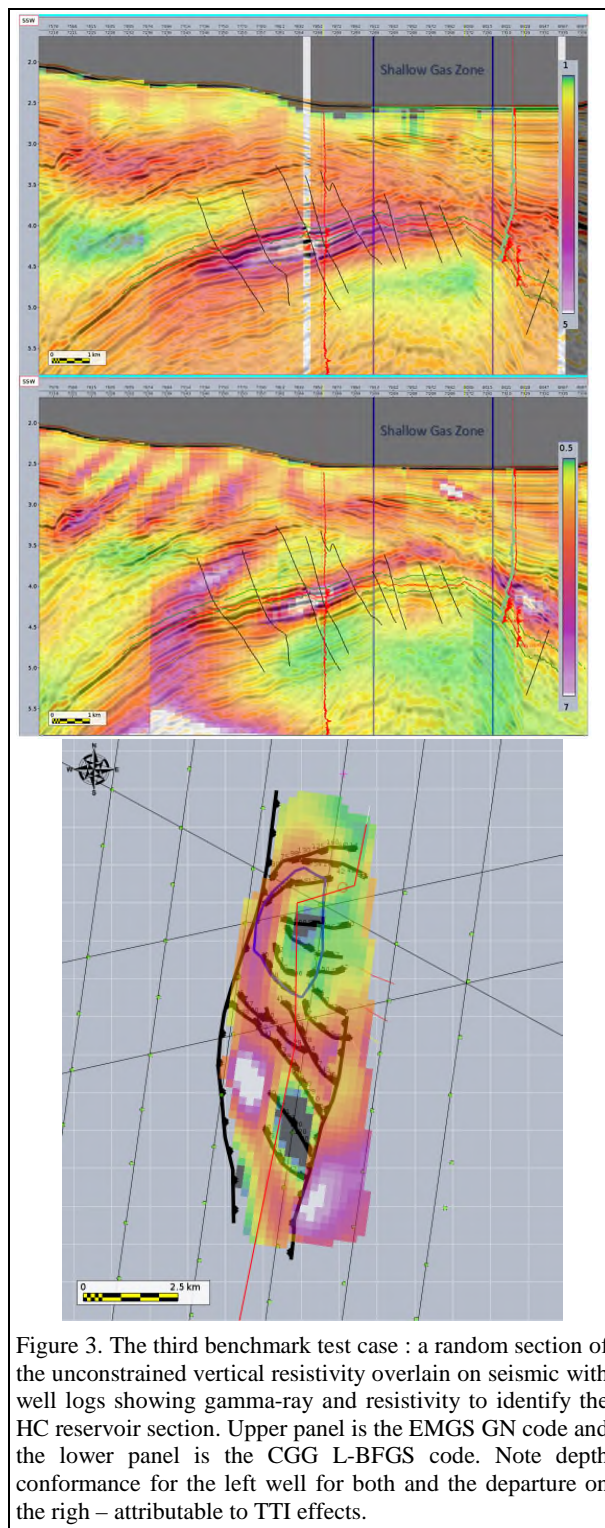

Figure 3. The third benchmark test case : a random section of the unconstrained vertical resistivity overlain on seismic with well logs showing gamma-ray and resistivity to identify the HC reservoir section. Upper panel is the EMGS GN code and the lower panel is the CGG L-BFGS code. Note depth conformance for the left well for both and the departure on the righ – attributable to TTI effects.

Each of these benchmark case studies will also be subjected to a volumetric assessment, as is illustrated in Figure 4 where initial anomaly definition is statistically based on the resistivity distribution (again, data-driven), probability of success updated and volume estimates refined. These numbers will of course then be compared with the real field appraisals.

Conclusions

These early and arguably positive results are encouraging for our ongoing efforts to build a catalogue of CSEM 'benchmark' case studies that will be used to better appreciate and quantify success rates, context of application, potential pit-falls and best practice methodology for application and integration of CSEM in the exploration workflow.

More presently, even pessimistic assessment of the qualitative correlation with the well results approximately support the 80% published success rates. As intended, these lookback exercises have also help refine the methodology for building and assessing CSEM inversions and integration with other data for definitive results.

These results can clearly modify the probability of success in an exploration context, and work is ongoing to assess the ability of integrated CSEM/seismic interpretation to better estimate the volumes in place based on the size of the CSEM resistivity anomaly, which should be more strongly correlated to hydrocarbons in-place than seismic amplitudes alone.

This will allow not only address the risking but also the economic assessment prior to drilling. As a natural extension, some of the benchmark case studies have been deliberately selected to include sub-economic discoveries to better inform the workflow for specific volume definition.

It is hoped that this study and associated work will dispel any remaining doubts as to the benefits and value of integrated prospect de-risking using seismic *and* CSEM in exploration contexts.
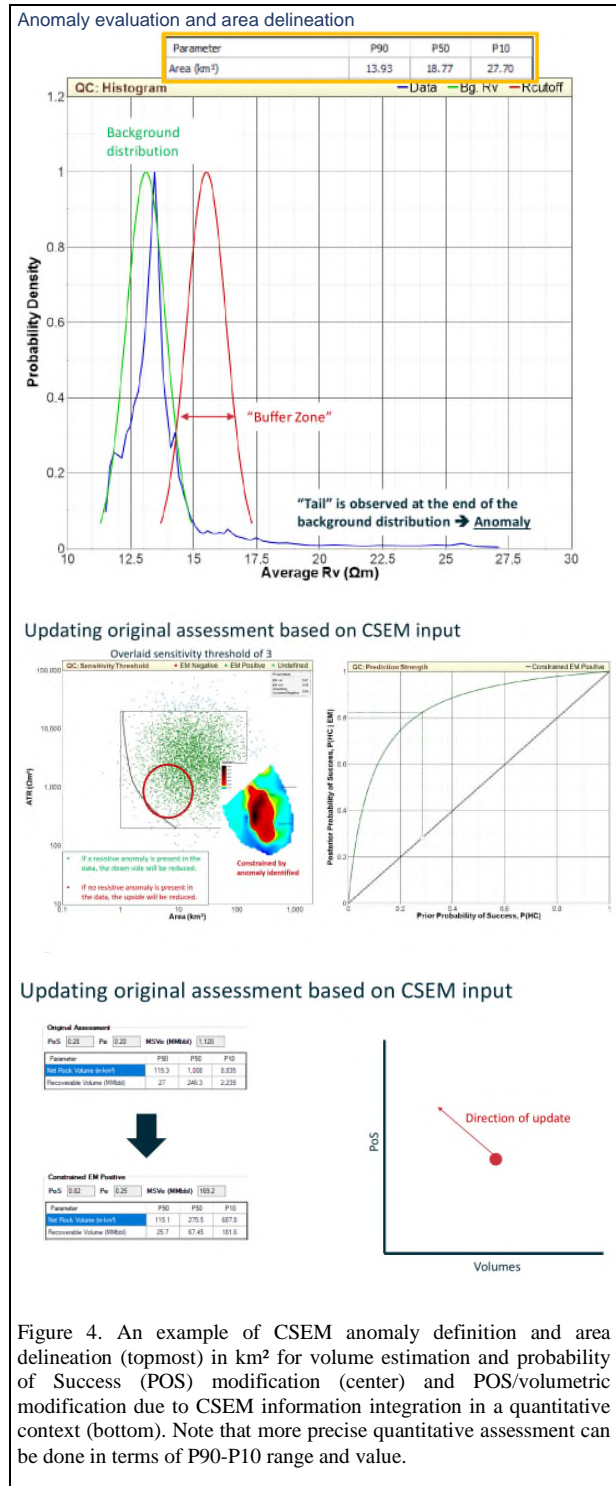
Acknowledgements

Figure 4. An example of CSEM anomaly definition and area delineation (topmost) in km² for volume estimation and probability of Success (POS) modification (center) and POS/volumetric modification due to CSEM information integration in a quantitative context (bottom). Note that more precise quantitative assessment can be done in terms of P90-P10 range and value.

REFERENCES

Eidesmo, T., S. Ellingsrud, L. M. MacGregor, S. Constable, M. C. Sinha, S. Johansen, F. N. Kong, and H. Westerdahl, 2002, Sea Bed Logging (SBL), a new method for remote and direct identification of hydrocarbon filled layers in deepwater areas: First Break, **20**, 144–152.

Hesthammer, J., A. Stefatos, and S. Sperrevik, CSEM efficiency-evaluation of recent drilling results: First Break, **30**, doi: https://doi.org/10.3997/1365-2397.2012007.

Rodi, W., and R. L. Mackie, 2001, Nonlinear conjugate gradients algorithm for 2-D magnetotelluric inversion: Geophysics, **66**, 14–357, doi: https://doi.org/10.1190/1.1444893.